Hindawi Publishing Corporation
Mathematical Problems in Engineering
Volume 2014, Article ID 746379, 10 pages
http://dx.doi.org/10.1155/2014/746379

Research Article

Robust D-Stability Controller Design for a Ducted Fan Unmanned Aerial Vehicle

Xiao-lu Ren, Chang-hong Wang, and Guo-xing Yi

Space Control and Inertial Technology Research Center, Harbin Institute of Technology, Harbin 150001, China

Correspondence should be addressed to Guo-xing Yi; ygx@hit.edu.cn

Received 14 February 2014; Accepted 17 March 2014; Published 22 April 2014

Academic Editor: Weichao Sun

This paper deals with the aerodynamic modeling of a small ducted fan UAV and the problem of attitude stabilization when the parameter of the vehicle is varied. The main aerodynamic model of the hovering flight UAV is first presented. Then, an attitude control is designed from a linearization of the dynamic model around the hovering flight, which is based on the H_∞ output feedback control theory with D-stability. Simulation results show that such method has good robustness to the attitude system. They can meet the requirements of attitude control and verify further the feasibility of such a control strategy.

1. Introduction

The ducted fan unmanned aerial vehicle is a new popular UAV in the recent years. Almost all system forces and moments come from the ducted fan. This UAV with VTOL (vertical takeoff and landings) and hovering flight capability is shown in Figure 1.

The ducted fan UAV can be adapted to a variety of complex environments and complete difficult flight missions [1, 2]. It is small with a compact and flexible layout. It is capable of maneuvering in any angle in addition to the normal hover and vertical takeoff and landing capabilities; therefore it can complete some special tasks [3, 4]. The peripheral duct not only enables the fan to be effectively protected, but also provides some aerodynamic lift for the vehicle's flight. The experiments show that the ducted unique geometry can provide some aerodynamic lift for the vehicle [5].

Compared with ordinary fixed-wing aircraft, ducted fan UAV has such advantages.

(1) *Flexibility.* Fixed-wing aircraft needs ground support in takeoff and landing. So it cannot provide timely information assurance to combat team in the city and mountain area. The ducted fan UAV can do vertical takeoff and landing and hover to adapt to the complex environment of the city or mountain. It can hover and stare at the target and fly close to the building to provide the precision position of the target [6, 7].

(2) *Compact Structure and High Propulsive Force.* Compared with unmanned helicopter, in the same power consumption, the ducted fan will produce greater tension than isolated propeller with the same diameter. The ducted fan UAV has more compact structure, less drag. And its flight attitude is closer to fixed-wing aircraft. So it can fly faster than the equivalent helicopter.

(3) *Low Noise, More Concealment, and Better Security.* The propeller is placed in the ducted fan, which can obstruct the transmission of aerodynamic noise. So the noise intensity and propagation distance can be reduced to some extent. Meanwhile the engine is surrounded by the ducted fan, which can obstruct the engine's thermal radiation, and then the vehicle's thermal radiation characteristic can be reduced. So the ducted fan UAV has better concealment, which can provide better survivability to the vehicle in the battle.

Compared with traditional fixed-wing aircraft, the flow field distribution of the ducted fan UAV is more complex, which makes the vehicle's modeling difficult. The attitude control is the key problem in the ducted fan UAV control, and it will affect the vehicle's other actions. In the flight, because the vehicle's flow field is complex [8–13], the nonlinear effect is obvious [14–17], and these will be big problems in the vehicle's

Figure 1: Ducted fan UAV.

control. In references [18, 19], an evolutionary pinning control is put toward which is applied in unmanned aerial vehicle coordination. Reference [20] used a PID control method. The PID method has a simple control structure and a low calculation amount, but the parameter adjustment is too cumbersome, and it has a poor adaptability for the coupling between the axes. Reference [21] used a robust H_∞ method. The H_∞ control has good inhibitory effect on the outside interference, but it is conservative to the uncertainty of the system. Reference [22] used a feedback linearization method, which has a good antijamming capability, but complex calculations.

This paper uses H_∞ output feedback control with D-stability for ducted fan UAV attitude control system with parameter uncertainty. The status of the system may be difficult to observe in the practical engineering. So the output variable which can be observed is used as feedback variable in this paper. Therefore, the output feedback control system has good physical realizability. Using H_∞ control method can resolve the uncertainties of the system but cannot provide location information of the closed-loop poles. H_∞ control method used in this paper which is combined with regional pole assignment not only ensures the robustness of control system, but also places the poles of the closed-loop system in a specified region. Dynamic performance of the UAV can be satisfied. This controller is designed by solving a set of linear matrix inequalities. Simulation results show this controller not only guarantees the closed-loop system to be D-stable, but also achieves the given H_∞ disturbance index. The vehicle can meet the requirements of attitude control and has good practicality, which illustrates the effectiveness of the proposed method.

2. UAV Attitude Modeling

2.1. Rotor Aerodynamics. Compared with the fixed-wing aircraft, the ducted fan vehicle has a more complicated air environment. The modeling of the fan is the main difficulty to the modeling of the whole vehicle.

There are two theories to study the fan, the momentum theory, and the blade element theory. This paper uses the two theories above to present the fan's aerodynamics equations.

The thrust can be expressed as [23]

$$T_{\text{fan}} = (v_b - v_i) \cdot \frac{\rho \cdot \omega_r \cdot a \cdot n \cdot d \cdot R^2}{4}, \tag{1}$$

where ω_r represents angular velocity of rotor, ρ is free stream density, R is the radius of the rotor, a is rotor blade lift curve slope, n represents the number of rotor blades, d is the rotor blade chord, v_b represents the flow through the rotor, and v_i is rotor induced velocity. The far field velocity can be expressed as

$$|v| = \sqrt{v_x^2 + v_y^2 + (v_z - v_i)^2}. \tag{2}$$

The induced velocity can be now expressed as follows:

$$v_i = \frac{T}{2\rho\pi R^2 |v|}. \tag{3}$$

The airflow along the z-axis can be expressed as

$$v_b = v_z + \frac{1}{2}\omega_r R K_{\text{twist}}, \tag{4}$$

where K_{twist} is the twist of the blades.

2.2. Duct. The airflow tends to follow the direction of the duct contour due to the Coandă effect. As a result, the wake will have a larger area than that of a helicopter. Comparing with a traditional helicopter, the duct provides additional thrust which can be attributed to the pressure distributions above and below the propeller. As shown in [24], the total thrust is the sum of the propeller or fan thrust and the force experienced by the duct:

$$\begin{aligned} T &= T_{\text{fan}} + T_{\text{duct}}, \\ \frac{T_{\text{fan}}}{T} &= \frac{1}{2a_d}, \end{aligned} \tag{5}$$

where a_d represents the ratio between the area of the wake and the propeller disk area.

The force on the vehicle due to the ducted fan can now be expressed as

$$F_{\text{rotor}} = \begin{bmatrix} 0 \\ 0 \\ -T \end{bmatrix}. \tag{6}$$

The rotor twisting moment can be expressed as

$$M_{\text{rotor}} = \begin{bmatrix} 0 \\ 0 \\ -\dfrac{P}{\omega_r} \end{bmatrix}, \tag{7}$$

where P is rotor output power.

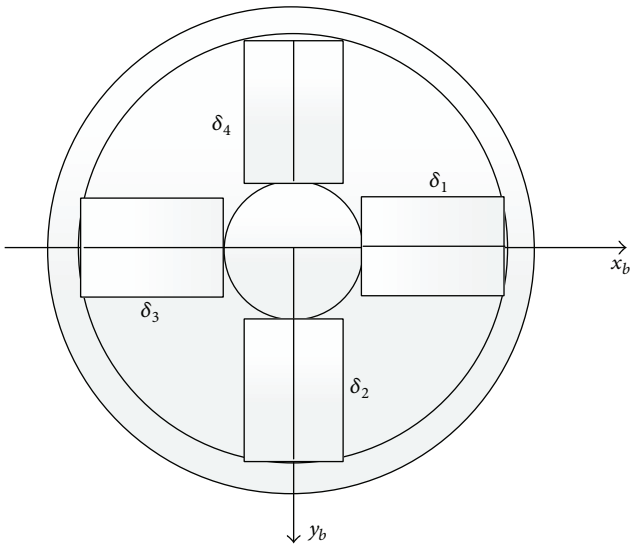

Figure 2: Configuration of control vane.

2.3. Control Vane. The rudder control torque is

$$L = \frac{1}{2}\rho v_i^2 S_r C_{Lr}(\delta),$$
$$D = \frac{1}{2}\rho v_i^2 S_r C_{Dr}(\delta), \tag{8}$$

where S_r is rudder surface area and C_{Lr}, and C_{Dr} are dimensionless lift coefficient and resistance coefficient, which are related to the deflection angle of the rudder.

The rudder surface distribution is shown in Figure 2; the control volume is $\delta_1 = \delta_p + \delta_r$, $\delta_2 = \delta_q - \delta_r$, $\delta_3 = \delta_p - \delta_r$, and $\delta_4 = \delta_q + \delta_r$, where δ_p, δ_q, and δ_r are roll, pitch, and yaw control volume and δ_1, δ_2, δ_3, and δ_4 are the deflection angles of the rudder.

2.4. Gyroscopic Moment. The expression for gyroscopic moment vector is given as

$$M_{\text{gyro}} = nI_b\omega_r \begin{bmatrix} -\omega_y \\ \omega_x \\ 0 \end{bmatrix}, \tag{9}$$

where I_b is the rotational inertia of the blade.

3. Modeling

The force and moment vectors can be expressed as

$$F = F_{\text{aero}} + F_{\text{rotor}} + F_{\text{vane}},$$
$$M = M_{\text{aero}} + M_{\text{rotor}} + M_{\text{vane}} + M_{\text{gyro}}. \tag{10}$$

The UAV dynamics and kinematics equations are given as

$$\begin{aligned}
\dot{v}_x &= -\left(v_z\omega_y - v_y\omega_z\right) + \frac{F_x}{m} - g\sin\theta,\\
\dot{v}_y &= -\left(v_x\omega_z - v_z\omega_x\right) + \frac{F_y}{m} - g\cos\theta\sin\phi,\\
\dot{v}_z &= -\left(v_y\omega_x - v_x\omega_y\right) + \frac{F_z}{m} - g\cos\theta\cos\phi,\\
I_{xx}\dot{\omega}_x &= \left(I_{yy} - I_{zz}\right)\omega_y\omega_z + I_{xz}\left(\dot{\omega}_z + \omega_z\omega_y\right) + M_x,\\
I_{yy}\dot{\omega}_y &= \left(I_{zz} - I_{xx}\right)\omega_z\omega_x + I_{xz}\left(\omega_z^2 - \omega_x^2\right) + M_y,\\
I_{zz}\dot{\omega}_z &= \left(I_{xx} - I_{yy}\right)\omega_x\omega_y + I_{xz}\left(\dot{\omega}_x + \omega_y\omega_z\right) + M_z,\\
\dot{\phi} &= \omega_x + \omega_y\sin\phi\tan\theta + \omega_z\cos\phi\tan\phi,\\
\dot{\theta} &= \omega_y\cos\phi - \omega_z\sin\phi,\\
\dot{\psi} &= \omega_y\sin\phi\sec\theta + \omega_z\cos\varphi\sec\theta,
\end{aligned} \tag{11}$$

where ϕ, θ, and ψ represent the vehicle roll, pitch, and yaw attitudes; ω_x, ω_y, and ω_z represent vehicle roll rate, pitch rate, and yaw rate; v_x, v_y, and v_z represent body-fixed velocity in the body-fixed x, y, z directions.

Hovering and low speed flight is the ducted fan UAV's main flight state. Using small perturbation theory and the Taylor expansion, the nonlinear equations of the system can be linearized:

$$\dot{x} = Ax + Bu,$$
$$y = Cx + Du, \tag{12}$$

where $x = [v_x, v_y, v_z, \omega_x, \omega_y, \omega_z, \phi, \theta, \psi]^T$, $u = [\delta_p, \delta_q, \delta_r]^T$, and δ_p, δ_q, and δ_r represent the control input.

3.1. Robust D-Stability Analysis in UAV Control System. Fully considering the uncertainty of the system, control object can be expressed as

$$\dot{x} = (A + \Delta A)x(t) + B_1\omega(t) + \left(B_2 + \Delta B\right)u(t),$$
$$z = C_1x(t) + Du(t),$$
$$y = C_2x(t), \tag{13}$$

where $x(t) \in R^n$ is the state vector of generalized object, $u(t) \in R^m$ is the control input, $\omega(t) \in R^p$ is the interference signal, $z(t) \in R^q$ is the output to adjust, $y(t) \in R^f$ is the output to measure, A is $n \times n$ real constant matrix, B_1 is $n \times p$ real constant matrix, B_2 is $n \times m$ real constant matrix, C_1 is $q \times n$ real constant matrix, D is $q \times m$ real constant matrix, C_2 is $f \times n$ real constant matrix, ΔA, ΔB represent the uncertainty of the real parameters in system state matrix and input matrix, $\left(\Delta A \;\; \Delta B\right) = HF\left(E_1 \;\; E_2\right)$, H, E_1, and E_2 represent the constant matrix which have the corresponding dimension, and F represents unknown matrices and meets $FF^T \leq I$.

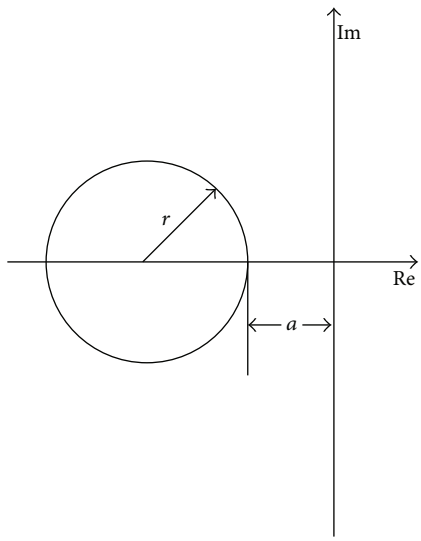

Figure 3: Region D.

Definition 1. Given performance index $\gamma > 0$, region $D(-q, r)$, as shown in Figure 3, the feedback controller (14) is said to be H_∞ output feedback controller with D-stability, if the following conditions are established.

(1) If the uncertainties of the control system meet $(\Delta A \;\; \Delta B) = HF(E_1 \;\; E_2)$ and $FF^T \leq I$, then the close-loop system is internal stability.

(2) The poles of the augmented closed-loop system are placed in region D shown in Figure 3.

(3) $\|T_{z\omega}\|_\infty$ is minimized, where $T_{z\omega}(s)$ is the closed-loop transfer function from ω to z; meanwhile, given $\gamma > 0$, $\|T_{z\omega}\|_\infty < \gamma$,

$$\begin{aligned} \dot{x}_c &= A_c x_c + B_c y, \\ u &= C_c x_c + D_c y. \end{aligned} \tag{14}$$

Augmented closed-loop system represents as

$$\begin{aligned} \dot{x}_{\mathrm{cl}} &= A_{\mathrm{cl}} x_{\mathrm{cl}} + B_{\mathrm{cl}} \omega, \\ z &= C_{\mathrm{cl}} x_{\mathrm{cl}}, \end{aligned} \tag{15}$$

where $x_{\mathrm{cl}} = (x \;\; x_c)^T$ is the state vector of the augmented closed-loop system and system matrixes are represented, respectively, as

$$\begin{aligned} A_{\mathrm{cl}} &= \begin{bmatrix} A + \Delta A + (B_2 + \Delta B) D_c C_2 & (B_2 + \Delta B) C_c \\ B_c C_2 & A_c \end{bmatrix}, \\ B_{\mathrm{cl}} &= \begin{bmatrix} B_1 \\ 0 \end{bmatrix}, \\ C_{\mathrm{cl}} &= [C_1 + D D_c C_2 \;\; D C_c]. \end{aligned} \tag{16}$$

Lemma 2. *Let U, W, and V be any given real matrixes which have the corresponding dimension. For a given symmetric matrix M, the following statements are equivalent.*

(1) *For any given matrix V which meets $V^T V \leq I$, U, W, and V satisfy*

$$M + UVW + W^T V^T U^T < 0. \tag{17}$$

(2) *There exists a real number $\varepsilon > 0$ which makes*

$$M + \varepsilon^{-1} U U^T + \varepsilon W^T W < 0. \tag{18}$$

Theorem 3. *Given upper bound $\gamma > 0$ and region $D(-q, r)$, for uncertainty system* (13)*, if there exists symmetric positive matrix $P = P^T > 0$ and real number $\varepsilon > 0$ for which*

$$\begin{bmatrix} N^* & B_{\mathrm{cl}} & P C_{\mathrm{cl}}^T & (\overline{A}_{\mathrm{cl}} + \alpha I) P & P \overline{E}^T & \varepsilon \overline{H} \\ B_{\mathrm{cl}}^T & -\gamma^2 & 0 & 0 & 0 & 0 \\ C_{\mathrm{cl}} P & 0 & -I & 0 & 0 & 0 \\ P(\overline{A}_{\mathrm{cl}} + \alpha I)^T & 0 & 0 & -rP & P \overline{E}^T & 0 \\ \overline{E} P & 0 & 0 & \overline{E} P & -\varepsilon I & 0 \\ \varepsilon \overline{H}^T & 0 & 0 & 0 & 0 & -\varepsilon I \end{bmatrix} < 0. \tag{19}$$

Then (1) *the poles of the augmented closed-loop system are placed in region $D(-q, r)$;* (2) *the close-loop system is stability internal and $\|T_{z\omega}\|_\infty < \gamma$, where*

$$\begin{aligned} \alpha &= q - r, \\ N^* &= (\overline{A}_{\mathrm{cl}} + \alpha I) P + P (\overline{A}_{\mathrm{cl}} + \alpha I)^T, \\ \overline{A}_{\mathrm{cl}} &= \begin{bmatrix} A + B_2 D_c C_2 & B_2 C_c \\ B_c C_2 & A_c \end{bmatrix}, \\ \overline{H} &= \begin{bmatrix} H & H \\ 0 & 0 \end{bmatrix}, \\ \overline{F} &= \begin{bmatrix} F & 0 \\ 0 & F \end{bmatrix}, \\ \overline{E} &= \begin{bmatrix} E_1 & 0 \\ E_2 D_c C_2 & E_2 C_c \end{bmatrix}. \end{aligned} \tag{20}$$

Proof. Consider

$$A_{\mathrm{cl}} = \overline{A}_{\mathrm{cl}} + \Delta A_{\mathrm{cl}}, \tag{21}$$

$$\begin{aligned}\Delta A_{\mathrm{cl}} &= \begin{bmatrix} \Delta A + \Delta B D_c C_2 & \Delta B C_c \\ 0 & 0 \end{bmatrix} \\ &= \begin{bmatrix} HFE_1 + HFE_2 D_c C_2 & HFE_2 C_c \\ 0 & 0 \end{bmatrix} = \overline{H}\,\overline{F}\,\overline{E},\end{aligned} \tag{22}$$

$$\begin{aligned}&\begin{bmatrix} N^* & B_{\mathrm{cl}} & PC_{\mathrm{cl}}^T & \left(\overline{A}_{\mathrm{cl}} + \alpha I\right)P \\ B_{\mathrm{cl}}^T & -\gamma^2 & 0 & 0 \\ C_{\mathrm{cl}}P & 0 & -I & 0 \\ P\left(\overline{A}_{\mathrm{cl}} + \alpha I\right)^T & 0 & 0 & -rP \end{bmatrix} \\ &+ \begin{bmatrix} \Delta A_{\mathrm{cl}}P + P\Delta A_{\mathrm{cl}}^T & 0 & 0 & \Delta A_{\mathrm{cl}}P \\ 0 & 0 & 0 & 0 \\ 0 & 0 & 0 & 0 \\ P\Delta A_{\mathrm{cl}}^T & 0 & 0 & 0 \end{bmatrix} < 0,\end{aligned} \tag{23}$$

$$\overline{Z} = \begin{bmatrix} N^* & B_{\mathrm{cl}} & PC_{\mathrm{cl}}^T & \left(\overline{A}_{\mathrm{cl}} + \alpha I\right)P \\ B_{\mathrm{cl}}^T & -\gamma^2 & 0 & 0 \\ C_{\mathrm{cl}}P & 0 & -I & 0 \\ P\left(\overline{A}_{\mathrm{cl}} + \alpha I\right)^T & 0 & 0 & -rP \end{bmatrix} \tag{24}$$

where (23) is equivalent to

$$\overline{Z} + \begin{bmatrix} \overline{H}\,\overline{F}\,\overline{E}P + P\left(\overline{H}\,\overline{F}\,\overline{E}\right)^T & 0 & 0 & \overline{H}\,\overline{F}\,\overline{E}P \\ 0 & 0 & 0 & 0 \\ 0 & 0 & 0 & 0 \\ P\left(\overline{H}\,\overline{F}\,\overline{E}\right)^T & 0 & 0 & 0 \end{bmatrix} < 0. \tag{25}$$

Then

$$\overline{Z} + \begin{bmatrix} \overline{H} \\ 0 \\ 0 \\ 0 \end{bmatrix} \overline{F} \begin{bmatrix} \overline{E}P & 0 & 0 & \overline{E}P \end{bmatrix} + \begin{bmatrix} P^T\overline{E}^T \\ 0 \\ 0 \\ P^T\overline{E}^T \end{bmatrix} \overline{F}^T \begin{bmatrix} \overline{H} & 0 & 0 & 0 \end{bmatrix} < 0. \tag{26}$$

Let

$$\overline{M} = \begin{bmatrix} \overline{H} \\ 0 \\ 0 \\ 0 \end{bmatrix}, \qquad \overline{N} = \begin{bmatrix} \overline{E}P & 0 & 0 & \overline{E}P \end{bmatrix}, \tag{27}$$

where (26) is equivalent to

$$\overline{Z} + \overline{M}\,\overline{F}\,\overline{N} + \overline{N}^T\overline{F}^T\overline{M}^T < 0. \tag{28}$$

According to Lemma 2, (25) is founded when all F meet $FF^T \le I$, only if there exists a positive constant ε, let

$$\overline{Z} + \varepsilon\overline{M}\,\overline{M}^T + \varepsilon^{-1}\overline{N}^T\overline{N} < 0. \tag{29}$$

Which is equivalent, by the Scher complement, to

$$\begin{bmatrix} \overline{Z} & \overline{N}^T & \overline{M} \\ \overline{N} & -\varepsilon I & 0 \\ \overline{M}^T & 0 & -\varepsilon^{-1}I \end{bmatrix} < 0. \tag{30}$$

Let inequality (30) premultiply and postmultiply $\mathrm{diag}\left(I \;\; I \;\; \varepsilon I\right)$.

The proof is completed. □

Since inequality (19) contains the nonlinear terms, it cannot be calculated directly by LMI. So the variable substitution should be performed to the inequality.

Lemma 4. *There exists symmetry positive definite matrix X; the necessary and sufficient condition that meets both* (31) *and* (32) *is*

$$X = \begin{bmatrix} R & M \\ M^T & * \end{bmatrix}, \tag{31}$$

$$X^{-1} = \begin{bmatrix} S & N \\ N^T & * \end{bmatrix}, \tag{32}$$

$$\begin{bmatrix} R & I \\ I & S \end{bmatrix} > 0. \tag{33}$$

Theorem 5. *Given H_∞ performance index $\gamma > 0$, positive real number ε, and region $D(-q, r)$, if there exist corresponding dimension real matrixes $R = R^T$ and $S = S^T$, matrixes $\widetilde{A}_c$, $\widetilde{B}_c$, $\widetilde{C}_c$, and $\widetilde{D}_c$ satisfy inequalities* (33) *and* (34)*:*

$$\begin{bmatrix} \Phi_{11} & \Phi_{12} & B_1 & \Phi_{14} & \Phi_{15} & \Phi_{16} & RE_1^T & \Phi_{18} & \varepsilon H & \varepsilon H \\ \Phi_{12}^T & \Phi_{22} & SB_1 & \Phi_{24} & \Phi_{25} & \Phi_{26} & E_1^T & \Phi_{28} & \varepsilon SH & \varepsilon SH \\ B_1^T & B_1^T S & -\gamma^2 I & 0 & 0 & 0 & 0 & 0 & 0 & 0 \\ \Phi_{14}^T & \Phi_{24}^T & 0 & -I & 0 & 0 & 0 & 0 & 0 & 0 \\ \Phi_{15}^T & \Phi_{25}^T & 0 & 0 & -rR & -rI & RE_1^T & \Phi_{18} & 0 & 0 \\ \Phi_{16}^T & \Phi_{26}^T & 0 & 0 & -rI & -rS & E_1^T & \Phi_{28} & 0 & 0 \\ E_1R & E_1 & 0 & 0 & E_1R & E_1 & -\varepsilon I & 0 & 0 & 0 \\ \Phi_{18}^T & \Phi_{28}^T & 0 & 0 & \Phi_{18}^T & \Phi_{28}^T & 0 & -\varepsilon I & 0 & 0 \\ \varepsilon H^T & \varepsilon H^T S & 0 & 0 & 0 & 0 & 0 & 0 & -\varepsilon I & 0 \\ \varepsilon H^T & \varepsilon H^T S & 0 & 0 & 0 & 0 & 0 & 0 & 0 & -\varepsilon I \end{bmatrix} < 0, \tag{34}$$

$$\Phi_{11} = AR + RA^T + B_2\widetilde{C}_c + \widetilde{C}_c^T B_2^T + 2\alpha R,$$

$$\Phi_{12} = A + \widetilde{A}_c^T + B_2\widetilde{D}_c C_2 + 2\alpha I,$$

$$\Phi_{22} = SA + A^T S + \widetilde{B}_c C_2 + C_2^T B_c^T + 2\alpha S,$$

$$\Phi_{14} = RC_1^T + \widetilde{C}_c^T D^T,$$

$$\Phi_{24} = C_1^T + C_2^T D_c^T D^T,$$

$$\Phi_{15} = AR + B_2\widetilde{C}_c + \alpha R,$$

$$\begin{aligned}\Phi_{16} &= A + B_2\widetilde{D}_c C_2 + \alpha I,\\ \Phi_{25} &= \widetilde{A}_c + \alpha I,\\ \Phi_{26} &= SA + \widetilde{B}_c C_2 + \alpha S,\\ \Phi_{18} &= \widetilde{C}_c^T E_2^T,\\ \Phi_{28} &= C_2^T \widetilde{D}_c^T E_2^T.\end{aligned} \tag{35}$$

Then all poles of the closed-loop system are placed within the circular region $D(-q, r)$, and the system is stable and $\|T_{z\omega}(s)\|_\infty < \gamma$.

Proof. By Lemma 4, there exists a symmetric positive definite matrix $P = \left[\begin{smallmatrix} R & M \\ M^T & U \end{smallmatrix}\right]$ and inverse matrix $P^{-1} = \left[\begin{smallmatrix} S & N \\ N^T & V \end{smallmatrix}\right]$, in which R, and S are symmetric positive definite matrixes, as $PP^{-1} = I$, and can get $MN^T = I - RS$; because $\left[\begin{smallmatrix} R & I \\ I & S \end{smallmatrix}\right] > 0$, then $I - RS$ is invertible and then M, and N are full-ranked; let

$$\begin{aligned}\Gamma_1 &= \begin{bmatrix} R & I \\ M^T & 0 \end{bmatrix},\\ \Gamma_2 &= \begin{bmatrix} I & S \\ 0 & N^T \end{bmatrix}.\end{aligned} \tag{36}$$

Obviously

$$\begin{aligned}P\Gamma_2 &= \Gamma_1,\\ \Gamma_2^T P \Gamma_2 &= \begin{bmatrix} R & I \\ I & S \end{bmatrix}.\end{aligned} \tag{37}$$

Then matrix $P = \Gamma_2 \Gamma_2^{-1}$; furthermore $P > 0$.

Let inequality (34) premultiply $\mathrm{diag}(\Gamma_2^T, I, I, \Gamma_2^T, I, I)$ and postmultiply $\mathrm{diag}(\Gamma_2, I, I, \Gamma_2, I, I)$.

We can have the following inequality:

$$\begin{bmatrix}
\Theta_{11} & \Theta_{12} & B_1 & \Theta_{14} & \Theta_{15} & \Theta_{16} & RE_1^T & \Theta_{18} & \varepsilon H & \varepsilon H \\
\Theta_{12}^T & \Theta_{22} & SB_1 & \Theta_{24} & \Theta_{25} & \Theta_{26} & E_1^T & \Theta_{28} & \varepsilon SH & \varepsilon SH \\
B_1^T & B_1^T S & -\gamma^2 I & 0 & 0 & 0 & 0 & 0 & 0 & 0 \\
\Theta_{14}^T & \Theta_{24}^T & 0 & -I & 0 & 0 & 0 & 0 & 0 & 0 \\
\Theta_{15}^T & \Theta_{25}^T & 0 & 0 & -rR & -rI & RE_1^T & \Theta_{18} & 0 & 0 \\
\Theta_{16}^T & \Theta_{26}^T & 0 & 0 & -rI & -rS & E_1^T & \Theta_{28} & 0 & 0 \\
E_1 R & E_1 & 0 & 0 & E_1 R & E_1 & -\varepsilon I & 0 & 0 & 0 \\
\Theta_{18}^T & \Theta_{28}^T & 0 & 0 & \Theta_{18}^T & \Theta_{28}^T & 0 & -\varepsilon I & 0 & 0 \\
\varepsilon H^T & \varepsilon H^T S & 0 & 0 & 0 & 0 & 0 & 0 & -\varepsilon I & 0 \\
\varepsilon H^T & \varepsilon H^T S & 0 & 0 & 0 & 0 & 0 & 0 & 0 & -\varepsilon I
\end{bmatrix} < 0, \tag{38}$$

where

$$\begin{aligned}\Theta_{11} &= AR + RA^T + B_2 D_c C_2 R + B_2 C_c M^T\\ &\quad + RC_2^T D_c^T B_2^T + MC_c^T B_2^T + 2\alpha R,\\ \Theta_{12} &= A + B_2 D_c C_2 + RA^T S + RC_2^T D_c^T B_2^T S\\ &\quad + RC_2^T B_c^T N^T + MC_c^T B_2^T S + MA_c^T N^T + 2\alpha I,\\ \Theta_{22} &= SA + A^T S + SB_2 D_c C_2 + NB_c C_2\\ &\quad + C_2^T B_c^T N^T + C_2^T D_c^T B_2^T S + 2\alpha S,\\ \Theta_{14} &= RC_1^T + RC_2^T D_c^T D^T + MC_c^T D^T,\\ \Theta_{24} &= C_1^T + C_2^T D_c^T D^T,\\ \Theta_{15} &= AR + B_2 D_c C_2 R + B_2 C_c M^T + \alpha R,\\ \Theta_{16} &= A + B_2 D_c C_2 + \alpha I,\\ \Theta_{25} &= SAR + SB_2 D_c C_2 R + NB_c C_2 R\\ &\quad + SB_2 C_c M^T + NA_c M^T + \alpha I,\\ \Theta_{26} &= SA + SB_2 D_c C_2 + NB_c C_2 + \alpha S,\\ \Theta_{18} &= RC_2^T D_c^T E_2^T + MC_c^T E_2^T,\\ \Theta_{28} &= C_2^T D_c^T E_2^T.\end{aligned} \tag{39}$$

Since the inequality contains the nonlinear terms, the variable substitution should be performed.

Define variable substitution as

$$\begin{aligned}\widetilde{A}_c &= SAR + NA_c^T M^T + SB_2 C_c M^T + SB_2 D_c C_2 R + NB_c C_2 R,\\ \widetilde{B}_c &= SB_2 D_c + NB_c,\\ \widetilde{C}_c &= C_c M^T + D_c C_2 R,\\ \widetilde{D}_c &= D_c.\end{aligned} \tag{40}$$

Substitutioning inequality (40) into inequality (38) results in inequality (34). The proof is completed. □

3.2. Robust D-Stability Dynamic Output Feedback Controller Design. Based on the above analysis, the nonlinear inequalities are converted to linear inequalities by variable substitution. From Theorem 5, for the system with parameter uncertainty, given H_∞ performance index $\gamma > 0$, positive real number $\varepsilon > 0$, and circular region $D(-q, r)$, then the output feedback controller with H_∞-D stability is designed as follows.

(1) Get a feasible solution of linear matrix inequalities R, S, $\widetilde{A}_c$, $\widetilde{B}_c$, $\widetilde{C}_c$, and $\widetilde{D}_c$.

(2) Verify that the matrix $I - RS$ is reversible. If reversible, make full rank decomposition where $MN^T = I - RS$.

(3) According to variable substitution equation (40), we can get

$$D_c = \widetilde{D}_c,$$
$$C_c = \left(\widetilde{C}_c - \widetilde{D}_c C_2 R\right) M^{-T},$$
$$B_c = N^{-1}\left(\widetilde{B}_c - SB_2\widetilde{D}_c\right),$$
$$A_c = N^{-1}\left[\widetilde{A}_c - S\left(A + B_2\widetilde{D}_c C_2\right)R\right]M^{-T} - B_c C_2 R M^{-T} - B_c C_2 R M^{-1} S B_2 C_c, \tag{41}$$

where (A_c, B_c, C_c, D_c) is the output feedback controller.

3.3. Simulation of Ducted Fan UAV Attitude Control. Based on the above model, the dynamic output feedback controller of the closed-loop system can be built. According to Theorem 5, the reconstruction of control law of systems is designed to place the closed-loop system poles into the circle region $D(-5, 4.5)$; let $\gamma = 0.92$, $\varepsilon = 1$.

Perturbation parameters $H = \begin{bmatrix}0.5 & 0.5 & 0.5 & 0.5 & 0.5 & 0.5 & 0.5 & 0.5 & 0.5\end{bmatrix}^T$ and $\begin{pmatrix}E_1 & E_2\end{pmatrix} = \begin{bmatrix}0.1 & 0.1 & 0.1 & 0.1 & 0.1 & 0.1 & 0.1 & 0.1 & 0.1 & 0.1 & 0.1 & 0.1\end{bmatrix}$.

Then satisfy $F^T(t)F(t) \leq I$, according to previous methods, the matrixes in control law reconfigurable systems are

$$A_c = \begin{bmatrix} -22.64 & -0.2732 & -0.09441 & -1.568 & -0.4542 & -0.2776 & 0.5601 & 0.601 & 0.1774 \\ 0.06462 & -8.671 & 0.6483 & 16.53 & 15.78 & 3.741 & 0.5845 & 1.741 & 0.7923 \\ -0.8520 & -2.610 & -0.8109 & 5.448 & -0.1541 & 0.8185 & -0.9721 & 0.3199 & 0.3014 \\ 1.983 & 5.107 & 2.086 & -11.26 & 6.820 & -0.9133 & 0.8767 & -0.1671 & -0.5441 \\ -2.984 & 0.04552 & -3.048 & -1.52 & -23.44 & -2.365 & -1.378 & -0.9767 & 0.06624 \\ -7.701 & 2.591 & -5.136 & -10.90 & -23.26 & -3.992 & -0.2918 & -0.5453 & -0.4525 \\ -6.050 & 476.2 & 28.74 & 93.85 & 171.2 & 38.17 & -1.440 & 10.07 & 8.601 \\ 114.2 & -590.1 & -39.47 & -118.6 & -239.3 & -50.20 & -0.7837 & -14.37 & -10.601 \\ -19.19 & -2.605 & -17.23 & -19.65 & -50.55 & -5.615 & -0.6332 & -1.285 & -1.281 \end{bmatrix},$$

$$B_c = \begin{bmatrix} -0.02361 & -0.01612 & -0.2993 & -0.1272 & -0.1637 & -0.9465 & 0.04412 & 0.3329 & -0.3412 \\ 0.1168 & -0.3121 & 0.1372 & 0.9954 & 0.4566 & 0.8167 & 0.8109 & -0.4101 & -0.2643 \\ -0.04551 & -0.04553 & -0.6308 & 0.4096 & -0.7956 & 0.4148 & -01628 & 0.4089 & 0.9448 \\ -0.03100 & 0.1068 & -0.1281 & -0.7726 & 0.3786 & -0.3129 & 0.3200 & -0.1454 & -0.2687 \\ -0.03587 & -0.09831 & -0.3434 & -0.9012 & -0.5590 & -0.1777 & -0.7323 & 0.7785 & -0.1931 \\ 0.5540 & -0.2112 & 0.4984 & 0.3361 & 0.8961 & -0.5204 & -0.7233 & 0.3424 & 0.5452 \\ 1.985 & -110.9 & 3.859 & 16.64 & 4.160 & 15.07 & -29.60 & -3.180 & -2.672 \\ -9.969 & 137.8 & -4.437 & -19.92 & -4.290 & -17.78 & 36.75 & 4.460 & 3.364 \\ 1.338 & 0.9083 & -2.200 & -0.2673 & 1.703 & -0.3880 & 2.000 & 0.7796 & 1.650 \end{bmatrix}, \tag{42}$$

$$C_c = \begin{bmatrix} 301.8 & -4.545 & 10.80 & 51.19 & 95.25 & 15.79 & -6.855 & -6.062 & -1.385 \\ -297.4 & 4.901 & -4.647 & -46.91 & -48.35 & -11.11 & 9.613 & 8.017 & 1.247 \\ 0.4401 & 3.211 & 0.2304 & -7.527 & -3.683 & -1.338 & -0.1323 & -0.5338 & -0.3353 \end{bmatrix},$$

$$D_c = \begin{bmatrix} 1.320 & 0.7305 & 1.317 & 0.6735 & 6.697 & 0.4660 & -0.3071 & -0.8931 & 0.3908 \\ -0.4978 & 0.4364 & 1.101 & 0.9777 & 5.969 & 0.3108 & 0.6912 & 0.3042 & 0.05631 \\ -0.3687 & 0.9844 & -0.2012 & -4.332 & -0.8031 & -3.081 & 0.9728 & 0.04252 & 0.09001 \end{bmatrix}.$$

Closed-loop poles distribution as shown in Figure 4.

As shown in Figure 4, in $F^T(t)F(t) \leq I$, the closed-loop system poles can be placed in a designated region within the left half-plane of the complex plane. Zero input response is displayed in Figures 5, 6, 7, 8, 9, and 10 which show that each state of the closed-loop system can quickly converge to zero. The system is asymptotically stable. Before and after the parameters change, the system's dynamic response curve

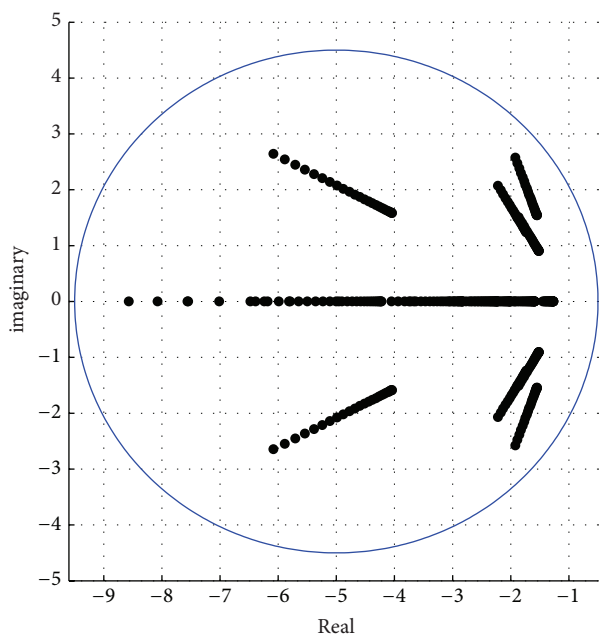

Figure 4: Closed-loop pole of the UAV control system.

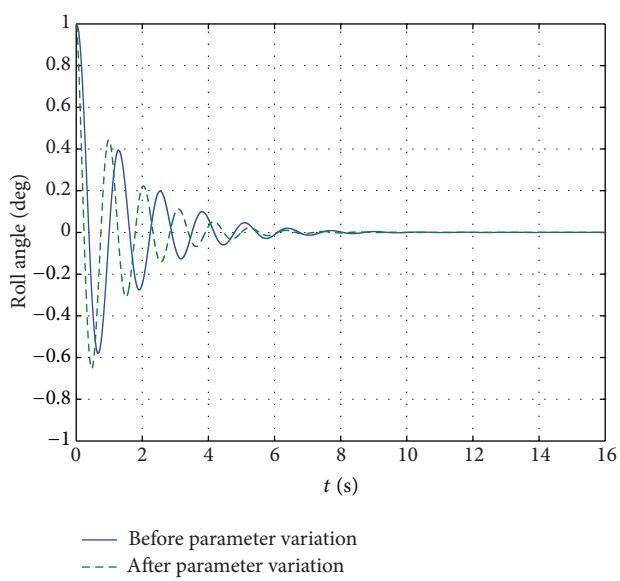

Figure 5: Response curve of roll angle before and after parameter variation.

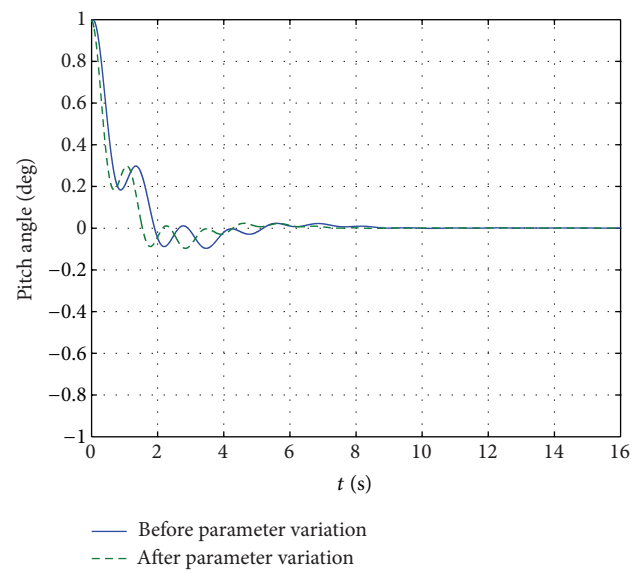

Figure 6: Response curve of pitch angle before and after parameter variation.

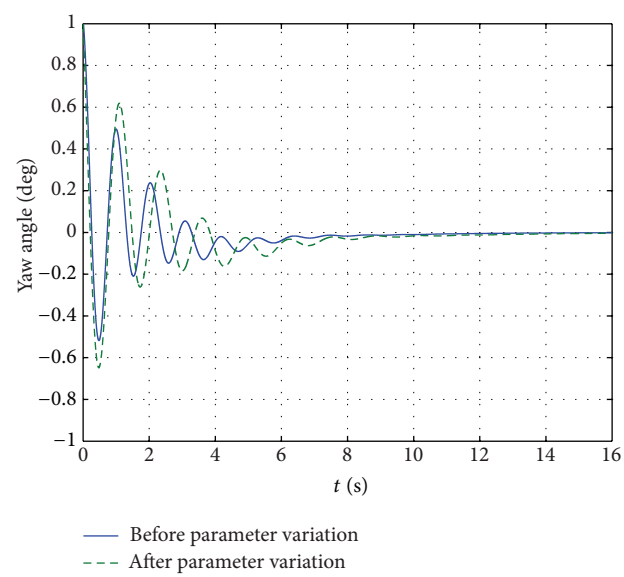

Figure 7: Response curve of yaw angle before and after parameter variation.

does not change significantly. The above results show that the dynamic output feedback controller effectively solves the system's uncertainty problem.

From the simulation results in Figures 5–10, three-axis attitude angle and angular velocity can quickly maintain stability with strong robustness. The ducted fan UAV has system uncertainty during the flight. As can be seen from the response curve before and after the load chance, in the presence of uncertainty, system poles can be maintained within the designated region and has good stability and dynamic performance.

4. Conclusion

This paper has established the ducted fan UAV's mathematical model and proposed a H_∞-D stabilization control method for linear uncertainty. This method gives the condition that meets both the interference suppression index constraints and regional pole constraints, in the form of linear matrix inequality (LMI).

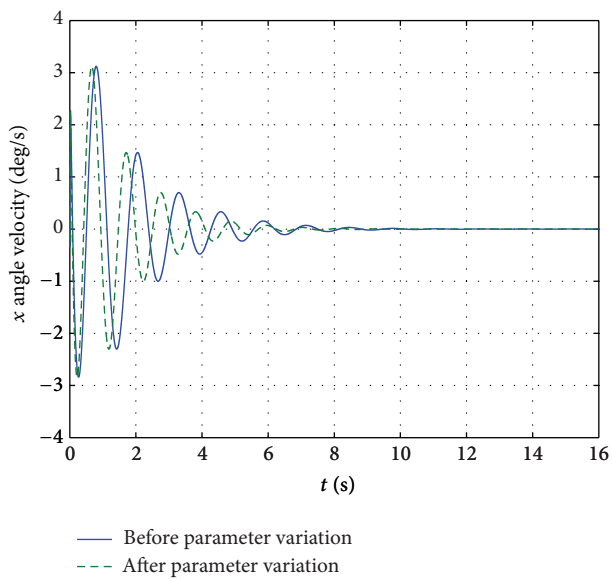

Figure 8: Response curve of x angle velocity before and after parameter variation.

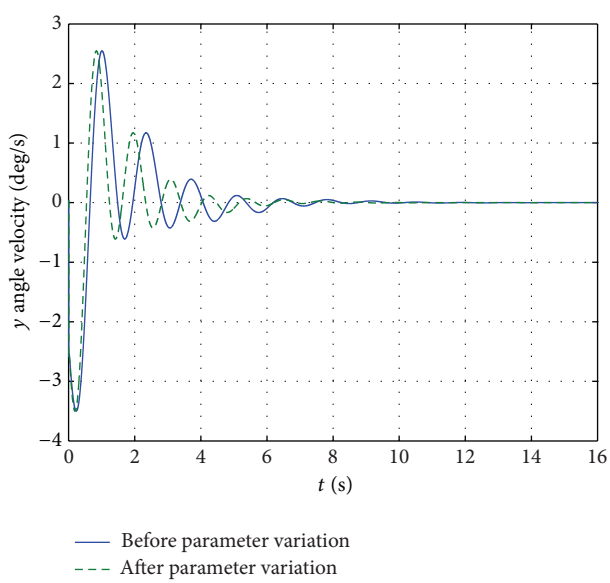

Figure 9: Response curve of y angle velocity before and after parameter variation.

This control method is applied in the ducted fan UAV's attitude control system. The simulation results demonstrate the effectiveness of this method. The experimental results show that this method has good robustness for both model linear uncertainty and controller uncertainty. This method can effectively suppress the crosswind interference to the control system. The regional pole constraints also give the system a good dynamic performance.

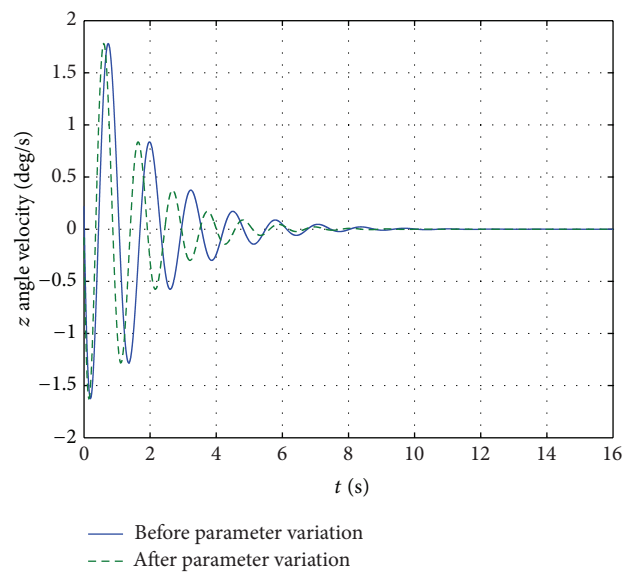

Figure 10: Response curve of z angle velocity before and after parameter variation.

Conflict of Interests

There is no conflict of interests regarding the publication of this paper.

References

[1] G. C. Ruzicka, R. C. Strawn, and E. T. Meadowcroft, "Discrete-blade, Navier-Stokes computational fluid dynamics analysis of Ducted-Fan flow," *Journal of Aircraft*, vol. 42, no. 5, pp. 1109–1117, 2005.

[2] A. Akturk, A. Shavalikul, and C. Camci, "PIV measurements and computational study of a 5-inch ducted fan for V/STOL UAV applications," in *Proceedings of the 47th AIAA Aerospace Sciences Meeting*, Orlando, Fla, USA, January 2009.

[3] E. N. Johnson and M. A. Turbe, "Modeling, control, and flight testing of a small ducted-fan aircraft," *Journal of Guidance, Control, and Dynamics*, vol. 29, no. 4, pp. 769–779, 2006.

[4] W. Haiming and W. Huaming, *A General Summarize for the Ducted Fan Computational Methods*, Institute of Helicopter Technology, Nanjing University of Aeronautics and Astronautics.

[5] X. Zhang, A. Myklebust, and P. Gelhausen, "A geometric modeler for the conceptual design of ducted fan UAVs," in *Proceedings of the AIAA 3rd Unmanned Unlimited Technical Conference*, AIAA 2004-6538, pp. 705–714, Chicago, Ill, USA, September 2004.

[6] J. K. Lee, D. H. Lee, and S. Kwon, "Performance prediction and design of a ducted fan system," in *Proceedings of the 40th AIAA/ASME/SAE/ASEE Joint Propulsion Conference*, AIAA 2004-4196, Fort Lauderdale, Fla, USA, July 2004.

[7] T. Wright, "Evaluation of the design parameters for optimum heavily loaded ducted fans," *Journal of Aircraft*, vol. 7, no. 6, pp. 512–517, 1970.

[8] I. Guerrero, K. Londenberg, P. Gelhausen, and A. Myklebust, "A powered lift aerodynamic analysis for the design of ducted fan UAVs," in *Proceedings of the 2nd AIAA Unmanned Unlimited*

Systems, Technologies, and Operations-Aerospace, AIAA 2003-6567, San Diego, Calif, USA, 2003.

[9] I. C. Chang and R. G. Rajagopalan, "CFD analysis for ducted fans with validation," in *Proceedings of the 21st Applied Aerodynamics Conference*, AIAA 2003-4079, Orlando, Fla, USA, 2003.

[10] O. J. Ohanian III, P. A. Gelhausen, and D. J. Inman, "A compact method for modeling the aerodynamics of ducted fan vehicles," in *Proceedings of the 48th AIAA Aerospace Sciences Meeting Including the New Horizons Forum and Aerospace Exposition*, Orlando, Fla, USA, January 2010.

[11] O. J. Ohanian III, E. D. Karni, W. Kelly Londenberg, P. A. Gelhausen, and D. J. Inman, "Ducted-fan force and moment control via steady and synthetic jets," in *Proceedings of the 27th AIAA Applied Aerodynamics Conference*, San Antonio, Tex, USA, June 2009.

[12] J.-M. Pflimlin, P. Binetti, P. Souères, T. Hamel, and D. Trouchet, "Modeling and attitude control analysis of a ducted-fan micro aerial vehicle," *Control Engineering Practice*, vol. 18, no. 3, pp. 209–218, 2010.

[13] L. Marconi, R. Naldi, and L. Gentili, "Modelling and control of a flying robot interacting with the environment," *Automatica*, vol. 47, no. 12, pp. 2571–2583, 2011.

[14] R. Naldi and L. Marconi, "Optimal transition maneuvers for a class of V/STOL aircraft," *Automatica*, vol. 47, no. 5, pp. 870–879, 2011.

[15] I. K. Peddle, T. Jones, and J. Treurnicht, "Practical near hover flight control of a ducted fan (SLADe)," *Control Engineering Practice*, vol. 17, no. 1, pp. 48–58, 2009.

[16] R. Naldi, L. Gentili, L. Marconi, and A. Sala, "Design and experimental validation of a nonlinear control law for a ducted-fan miniature aerial vehicle," *Control Engineering Practice*, vol. 18, no. 7, pp. 747–760, 2010.

[17] J. Yu, A. Jadbabaie, J. Primbs, and Y. Huang, "Comparison of nonlinear control design techniques on a model of the Caltech ducted fan," *Automatica*, vol. 37, no. 12, pp. 1971–1978, 2001.

[18] Y. Tang, H. Gao, W. Zou et al., "Distributed synchronization in networks of agent systems with nonlinearities and random switchings," *IEEE Transactions on Cybernetics*, vol. 43, no. 1, pp. 358–370, 2013.

[19] Y. Tang, H. Gao, J. Kurths et al., "Evolutionary pinning control and its application in UAV coordination," *IEEE Transactions on Industrial Informatics*, vol. 8, no. 4, pp. 828–838, 2012.

[20] H. J. Kim and D. H. Shim, "A flight control system for aerial robots: algorithms and experiments," *Control Engineering Practice*, vol. 11, no. 12, pp. 1389–1400, 2003.

[21] C.-D. Yang and W.-H. Liu, "Robust H_∞ decoupling hover control of uncertain nonlinear helicopter," in *Proceedings of the AIAA Guidance, Navigation, and Control Conference and Exhibit*, AIAA 2003-5489, pp. 3454–3459, Austin, Tex, USA, June 2003.

[22] O. Fritsch, P. De Monte, M. Buhl, and B. Lohmann, "Quasi-static feedback linearization for the translational dynamics of a quad rotor helicopter," in *Proceedings of the American Control Conference*, pp. P125–P130, 2012.

[23] E. N. Johnson and M. A. Turbe, *Modeling, Control, and Flight Testing of a Small Ducted Fan Aircraft*, Georgia Institute of Technology.

[24] A. D. Roberts, *Attitude Estimation and Control of a Ducted Fan VTOL UAV [M.S. thesis]*, Lakehead University, Thunder Bay, Ontario, Canada, 2007.